High-temperature plastic behavior of TZP-Ni cermets

A. Morales-Rodríguez, A. Bravo-León, A. Domínguez-Rodríguez[‡] and M. Jiménez-Melendo[†]

Departamento de Física de la Materia Condensada, Universidad de Sevilla. P. O. BOX 1065, 41080 Sevilla, Spain.

Abstract

The creep behavior of tetragonal zirconia TZP-Ni cermets with metal contents below, close to and above the percolation limit has been studied. Compressive creep tests were performed on as-received materials and samples in which the metal phase was chemically removed (ceramic skeletons). The stress exponent and the activation energy for plastic flow are independent of the nickel content and decrease continuously when increasing the stress and/or the temperature; skeleton structures display the same trend, suggesting that creep is controlled by the zirconia matrix. The steady-state constitutive equation for high-purity monolithic zirconia applies to the cermets when the stress is corrected with porosity and volume fraction of percolated nickel.

Keywords: cermet, TZP, nickel, creep, percolation

Supported by CICYT under projects No. MAT2000-1117 (Ministerio de Educación y Ciencia, Spain).

Based, in part, on the thesis submitted by A. Morales-Rodríguez for the PhD degree at the University of Seville, Seville, Spain, 2004.

[†] Corresponding author. E-mail address: melendo@us.es.

[‡] Fellowship in the American Ceramic Society.

1. Introduction

Nowadays there is a significant interest in the use of zirconia/nickel composites in multifunctional applications as temperature and flow sensors[1], thermal barriers coatings[2] and particularly anodes for solid oxide fuel cells (SOFCs)[3,4]; these cells operate at high temperatures in a reducing environment. TZP-Ni cermets offer a singular combination of electrical and mechanical properties; moreover, they are relatively inexpensive, chemically stable and immiscible with each other over a wide range of temperatures. The potential applications of these cermets require the study of their mechanical response, especially at high temperatures and over long-term operation, which is strongly affected by the microstructure: particle size, phase distributions, porosity, nature of grain boundaries, etc. A few studies devoted to explore the mechanical characteristics of the zirconia/nickel system at room temperature[5,6] concluded that the flexural resistance, elastic modulus, Vickers hardness and fracture strength decrease with increasing the nickel content. In a preliminary work[7], it was shown that the high-temperature mechanical behavior of TZP-Ni composites depends critically on the Ni volume fraction.

The percolation threshold for TZP-Ni cermets, measured by electrical conductivity and complex impedance measurements, corresponds to a nickel concentration of 34 vol%[8-10]; conduction is ionic below this value and electronic above it. This abnormally high percolation threshold (more than twice the value predicted by classical percolation theory in disordered systems)[10] has been correlated with a partial first-neighbor ordering of the metallic inclusions inside the ceramic matrix.

The aim of this study is to investigate the high-temperature mechanical behavior of wet-processed TZP-Ni cermets with metal concentrations below, close to and above the percolation threshold. Creep tests and microstructural studies were carried out and the results compared with the behavior of the skeletons structures (that is, cermets free of nickel) and that of TZP and polycrystalline nickel monoliths.

2. Experimental Procedure

The materials studied, provided by the ICMM (Instituto de Ciencias de Materiales de Madrid, Spain), were fabricated by a wet-processed route; a detailed description of the fabrication process can be found elsewhere[10]. The composites were prepared using a mixture of commercial powders of 3 mol% of yttria-stabilized ZrO_2 with an impurity content lower than 0.02 wt % and an average crystallite size of 60 nm (TZ-3YS; Tosoh Corp.) and ultrafine Ni with 99.9 wt % purity (NFP-401; Kawatetsu Mining Co., Ltd). Metallic particles formed welded aggregates ~ 1 μm in size, which controlled their final rheological behavior. Suspensions in distilled water were prepared with relative proportions of the metallic phase of 20, 30 and 40 vol% (hereafter referred to as Ni20, Ni30 and Ni40, respectively). After attrition milling with zirconia balls, the resultant powders were cold isostatically pressed into prismatic blocks of 4 x 4 x 40 mm^3 and sintered in reducing atmosphere (90% Ar/10% H_2) at 1430ºC for 2 h. Bulk densities were determined by measuring the dimensions and weight of the samples. Theoretical values were calculated by the rule of mixtures by taking ρ_{TZP} = 6080 kg/m^3 and ρ_{Ni} = 8900 kg/m^3.

Zirconia skeletons were obtained from the as-received composites to study the influence of the metallic phase in the plastic behavior. Nickel was chemically removed by etching with HNO_3 at room temperature for a maximum of 80 h; the process was controlled by weight measurements.

Rectangular specimens of about 3x3x4 mm^3 in size were cut from the as-received materials and deformed in compression under constant load in argon atmosphere to prevent nickel oxidation. The tests were carried out between 900 and 1250 ºC using nominal stresses between 9 and 144 MPa. The load was applied gradually at the beginning of the tests.

Data obtained from creep tests, instantaneous specimen length ℓ(t) versus time t, were reduced to true strain $\varepsilon = -ln\frac{\ell}{\ell_0}$, with ℓ_0 the initial length, and strain rate $\dot{\varepsilon} = -\frac{1}{\ell}\frac{\Delta\ell}{\Delta t}$ and plotted as log $\dot{\varepsilon}$ - ε curves (creep curves) for a better characterization of the steady-state regime.[11] These data were analyzed using the high-temperature creep equation for steady state:

$$\dot{\varepsilon} = A\sigma^n d^{-p}\, exp\left(-\frac{Q}{RT}\right) \quad (1)$$

where A is a constant, d the grain size, n the stress exponent, p the grain size exponent, Q the activation energy for plastic flow and R the gas constant. Stress and temperature changes were performed during the tests in order to calculate the apparent values of n and Q, respectively (differential method).

The microstructural characterization of the as-received and deformed composites was carried out using scanning (SEM) and transmission electron microscopy (TEM) (Microscopy Service-CITIUS, University of Seville, Spain) and high-resolution transmission (HRTEM) and analytical electron microscopy (Max-Planck Institute for Metal Research, Stuttgart, Germany). Sections for microscopy observations were cut from the samples and prepared following classical methods. The morphological parameters of both phases were measured by using a semiautomatic image analyzer.

3. Results

3.1. Microstructure of the as-received materials

The densities of the three as-received cermets were about 85% of the corresponding theoretical values; these values are 10-15% higher than those obtained conventionally from co-sintering of NiO and zirconia powders and subsequent reduction of NiO to metallic Ni[9,12]. Despite the zirconia facility to achieve fully-dense sintered-compacts at high temperatures, the addition of nickel prevents a fully densification of the TZP matrix[10].

Fig. 1 illustrates the microstructure of the as-received cermets. An exhaustive characterization has been reported elsewhere[13]. Briefly, the nickel phase (bright phase) is homogeneously distributed in the TZP matrix (gray phase) in the three cermets. Pores (black phase) are usually associated to nickel/zirconia interfaces. Zirconia grains are equiaxed with an average grain size (taken as the equivalent planar diameter $d = (4 \times \text{area} / \pi)^{1/2}$) of 0.13 μm. In Ni20 and Ni30, nickel inclusions are isolated from each other, with a round shape and a particle size of about 1 μm. In contrast, the metallic phase is interconnected in Ni40, in agreement with its nickel content above the percolation limit.

X-ray diffraction and TEM observations have shown that the TZP grains were stabilized in the tetragonal phase. HRTEM studies[13] revealed that zirconia/zirconia and zirconia/nickel interfaces, as well as triple grain junctions, are free of glassy phases. Moreover, segregation of yttrium to grain boundaries was observed with an enrichment factor of about 2. The same features have been reported previously in high-purity monolithic zirconia[14-16].

For the skeleton structures, residual nickel contents of 3, 5, and 5 (± 1 vol%) were estimated by weight measurements in Ni20, Ni30, and Ni40, respectively; the major loss of metal occurred within the first 20 h of chemical etching. Figure 2 shows SEM micrographs of Ni20 and Ni40 skeletons; the microstructure of Ni30 skeletons is intermediate between them. The residual metal is randomly distributed in the sample volume and corresponds to disconnected inclusions not accessible by open porosity.

3.2. High-temperature plastic deformation

The creep behavior of TZP-Ni cermets and skeletons has been studied in argon atmosphere to prevent nickel oxidation (a parallel study but in air has been reported elsewhere [17]); the zirconia phase is unaffected by the testing atmosphere[18]. Deformed cermets did not show any macroscopic sign of damage (Fig. 3), despite the large strains attained. In contrast, skeletons showed macroscopic flaws after deformation: cracking of edges and even catastrophic failure in the most severe deformation conditions.

(A) **Effect of nickel content:** Fig. 4 shows the creep curves for Ni20 (circles), Ni30 (triangles) and Ni40 (squares) recorded at low stresses (9-14 MPa) and temperatures between 1200 and 1250 ºC. Several features can be pointed out:

(i) Ni20 and Ni30 exhibit identical creep rates at the initial strain levels, though a larger strain rate for Ni30 could be expected because of its higher nickel content (nickel is less resistant than zirconia; see ‘‘Discussion’’);

(ii) The strain rate of Ni30 gradually increases with deformation compared with that of Ni20; the difference in strain rate increases consequently with the level of deformation. This observation was confirmed by dedicated tests at a fixed stress and temperature (Fig. 5). Such a behavior suggests that qualitative microstructural changes occur in Ni30 with strain, as confirmed later by SEM observations and electrical resistivity measurement[13];

(iii) Ni40 deforms at a much faster rate than the other two cermets in more than one order of magnitude; and

(iv) The mean values of n and Q measured from σ and T sudden changes during the tests are very similar in the three materials: $n = 4.0 \pm 0.4$ and $Q = 620 \pm 30$ kJ·mol^{-1} in Ni20; $n = 3.8 \pm 0.5$ and $Q = 670 \pm 60$ kJ·mol^{-1} in Ni30; $n = 3.9 \pm 0.1$ and $Q = 640 \pm 40$ kJ·mol^{-1} in Ni40. The lack of dependence in the creep parameters with nickel content was also found at other temperatures and stresses (Tables I and II).

(B) **Effect of stress and temperature:** In order to investigate a possible evolution of the creep parameters n and Q with stress and temperature in the cermets (as found in monolithic zirconia[19]), a series of creep tests at fixed stress or temperature were carried out. Tables I and II summarize the values of n and Q obtained for the three cermets at the different conditions studied. It was found that, at a given temperature, both n and Q

decrease with increasing the stress. In Ni20, for example, values of n = 4.0 ± 0.4 and Q = 620 ± 30 kJ·mol^{-1} were measured at low stresses (9-14 MPa, Fig. 4), which decreased to 3.5 ± 0.2 and 550 ± 40 kJ·mol^{-1} at moderate stresses (15 - 25 MPa) and to 2.8 ± 0.3 and 490 ± 50 kJ·mol^{-1} at higher stresses (32 - 66 MPa).

Similarly, both n and Q values increase when decreasing the temperature at a given stress (Tables I and II). Ni40, for instance, exhibits n = 3.5 ± 0.2 and Q = 550 ± 30 kJ·mol^{-1} at 1250 ºC, increasing up to 4.9 ± 0.3 and 660 ± 50 kJ·mol^{-1} at 1150 ºC (Fig. 6).

These trends, i.e., n and Q that decrease when increasing the stress and/or the temperature, are characteristic of pure monolithic zirconia[19], suggesting that this phase primarily controls the overall creep behavior of TZP-Ni cermets.

It is worth mentioning the high ductility exhibited by the cermets even at the lower temperatures studied (900-950 ºC), especially Ni40, which was deformed up to ε = 50% without any macroscopic signal of degradation.

(C) Creep of skeleton structures: The role of the metal phase in the cermets' plasticity has been investigated by testing their ceramic skeleton structures under similar experimental conditions. Ni20- and Ni30-skeletons deform at somewhat higher strain rates than their composite parents, while Ni40 skeletons behave identically, regardless of the stress and temperature conditions; Fig. 7 illustrates this behavior for Ni30 and Ni40. The values of n and Q measured for the skeletons are identical to those found in the cermets, suggesting again that zirconia controls the strain rates in the composite.

The elimination of the metallic phase in these structures led, however, to a decline in ductility, especially at the lower temperatures studied, where the skeletons failed catastrophically after strains of about 15%.

3.3. Microstructure of deformed materials

Fig. 8 illustrates typical microstructures of deformed cermets. A detailed microstructural characterization has been reported previously[13]. Nickel particles elongate during the deformation process, with the largest diameter perpendicular to the loading direction; this change in shape promotes the contact between neighbor inclusions. This contact is reflected in an apparent increase of the nickel particle size in deformed Ni30 and Ni40 cermets with respect to the as-received characteristics. This feature is critical in Ni30, where the nickel content is below but very close to the percolation threshold (34 vol%). On the other hand, zirconia grains did not undergo any significant change. An inhomogeneous redistribution of the metallic phase throughout the matrix was observed in Ni30 and Ni40 cermets after deformation, giving rise to metal-free regions; the number and size of these metal-free areas increase with increasing nickel content[13].

Densification took place during the creep process. The final density depends on the nickel content, creep conditions, and final strain. On average, the final densities were 90% ± 2% of the theoretical values, except at the highest temperature (1250 °C) and the lowest stress (3 MPa) studied, where the final density increased up to 95%. Densification took place especially upon application of load at the beginning of the tests, as evidenced by the very

large negative slopes α of the log $\dot{\varepsilon}$ - ε plots[‡] at the first few percents of strain.[7] Although densification was unavoidable during the rest of the tests, the maintenance of the strain rate levels after positive and negative changes in experimental conditions (Figs. 4, 6, and 7), along with the rough agreement of the values of a with the apparent n, suggests that it slowed down with respect to the initial densification. Regarding the ceramic skeletons, a similar densification process can be assumed because of their similar creep curves (Fig. 7) with respect to the parent cermets.

TEM and HRTEM studies showed the same features noted above for as-received materials: absence of dislocation activity inside the grains and of secondary phases at the interfaces and multiple grain junctions[13].

Cermets deformed at the higher stresses and lower temperatures developed cavities along TZP grain boundaries (Fig. 9), which occasionally coalesced into microcracks perpendicular to the compression axis without apparent worsening of the creep behavior (at least, up to strains of 50%).

4. Discussion

The monolithic parent phases of the cermets, Ni and TZP, behave very differently in the experimental conditions used in this work. The creep parameters of monolithic nickel are n = 1 and Q = 115 kJ·mol^{-1}, associated with Coble creep: they increase towards 5 and 280 kJ·mol^{-1}, respectively, when increasing σ and/or T due to the contribution of a dislocation

[‡] It can be easily shown from Eq. (1) that the slope a of the log $\dot{\varepsilon}$ - ε plot in the steady state is equal to -n, the apparent stress exponent measured by stress changes, under the assumption of homogeneous deformation.

recovery creep mechanism[20]. Typical strain rates are above 10^{-2} s^{-1} in similar conditions, significantly higher than those of the cermets.

On the other hand, monolithic TZP exhibits superplasticity at temperatures $T \geq 1100$ ºC, associated with grain boundary sliding. Creep parameters display a complex variation with stress, temperature, grain size and material purity[19, 21]; for high-purity zirconia, n and Q increase continuously from 2 to 5 and from 500 to 700 $kJ \cdot mol^{-1}$ when decreasing the stress and/or temperature[19]. The atomistic mechanisms responsible for this evolution are still in discussion. Typical creep rates range from 10^{-6} to 10^{-4} s^{-1} in the experimental conditions used in this study.

The values of n and Q found in the three cermets, along with their evolution with σ and T (Tables I and II), are very similar to those reported for high-purity monolithic zirconia, suggesting that the overall mechanical behavior of the composites is primarily controlled by the ceramic phase through a grain boundary sliding mechanism. This conclusion is also supported by: (i) the independence of n and Q with the metal content (Fig. 4); and (ii) the cermets and their associated skeletons exhibit identical values of n and Q (Fig. 7). A hard-phase control of the high-temperature plastic deformation has been also proposed in other cermets: $BaCe_{0.8}Y_{0.2}O_{3-y}$/Ni [22], TiMoCN-Ni/Co [23] and SiC/Si [24].

Assuming that the zirconia is the rate-controlling phase in the cermets, it is now possible to compare the strain rates of the composites with that of monolithic zirconia. Owen and Chokshi[25] have demostrated that the deformation mechanisms in porous (initial densities of 60%–77%) and fully dense TZP are identical. In order to minimize the effect of

densification on the creep rates, only the first stages of each creep curve have been taken into account in the analysis that follows; data for the highest temperature and lowest stresses have not been considered. Moreover, the corresponding strain rates have been extrapolated to $\varepsilon = 0$, which adequately corrects for densification as well as for the increase of sample section during deformation.

Fig. 10 displays the variation of grain size-compensated strain-rate at $\varepsilon = 0$, $\dot{\varepsilon}_0$, with σ at 1250ºC; a grain size exponent p = 2 [19] has been used to normalize the strain rates. A few results on monolithic zirconia produced by the same route as the cermets are also plotted in Fig. 10, along with data for high-purity zirconias[25, 26]; the n = 2 behavior of TZP is also shown.[19] Ni20 and Ni30 deform faster than monolithic TZP by a factor of 3; the difference with Ni40 is remarkably higher, a factor of 60. It should be noted that the differences in strain rate between cermets and skeletons are unmodified by the choice of p because all of them have the same grain size.

In a preliminary work focused on Ni20 and Ni40[7], it was shown that the creep rates of the cermets could not be explained by simple isostrain or isostress creep models for duplex microstructures[26]. A new approach is presented here in the framework of the stress-porosity model based on the minimum solid area (MSA) proposed by Rice[28, 29] to describe the mechanical properties of porous materials. In the MSA models, the mechanical properties depend on the weakest zone of the solid structure: the zone with minimum solid area supports the maximum stress and thereby, the minimum area perpendicular to the applied stress controls the stress transmission in the material. The MSA of a particular

microstructure depends on the topology of the pores, as well as on the type of stacking and amount of porosity.

The three cermets studied have a nickel content well below (Ni20), close to (Ni30), and higher (Ni40) than the critical value for percolation. The metal inclusions are isolated from each other in Ni20 and Ni30, surrounded by zirconia grains; nickel particles are therefore blocked out from deforming as in monolithic nickel. The metal phase can then be considered as an incompressible phase forced to be contained in a fixed volume. Interfacial effects can also be neglected because of the very weak metal/ceramic bonding in these cermets[31, 32].

Within this frame, a uniaxial stress applied on Ni20 and Ni30 (in this last case, at the early steps of deformation) will be redistributed at the interfaces of the nickel inclusions, changing their equiaxed shape to a flattened form. That is, the same stress will act on the ceramic phase –which controls the plastic behavior– in both Ni20 and Ni30 despite their different metal content. This is consistent with the identical values of $\dot{\varepsilon}$ experimentally found in Ni20 and Ni30 in the first steps of deformation (Figs. 4 and 5) and the elongation of nickel particles during the creep process (Fig. 8).

The behavior of the metal phase in Ni40 is remarkably different because it is already percolated. The interconnection of the nickel particles makes possible that nickel flows from regions in compression to those in tension without offering any resistance to creep. The experimental features are consistent with this idea: (i) identical creep rates of Ni40 and its skeleton (Fig. 7); (ii) nickel-defective areas were commonly observed in Ni40 and were

also present in Ni30[13]; and (iii) the raise of $\dot{\varepsilon}$ in Ni30 with respect to Ni20 after a certain amount of deformation (Figs. 4 and 5) because of the increase in metal phase connectivity caused by the elongation of nickel. It is concluded therefore that the metal phase in the percolated cermet can be regarded as effective porosity with respect to its capability for carrying load.

For the MSA analysis, the cermets have been modeled by a cubic stacking of spherical pores, corresponding to the real porosity in Ni20 and Ni30 ($\varepsilon \leq 25\%$ have been considered for this latter case, Figs. 4 and 5, to avoid the onset of percolation) and the effective porosity (the real one plus the volume fraction of the metal phase) in Ni40, that is, the actual porosity of Ni40 skeletons. A real porosity of 10% has been used for the three cermets according to their final densities. The measured residual nickel content of each skeleton has also been taken into account in the calculations.

In this model, the applied stress σ in a cermet with porosity P is related to the actual stress acting on the zirconia phase σ_R by [29]:

$$\frac{\sigma}{\sigma_R} = 1 - \frac{\pi}{4}\left(\frac{6P}{\pi}\right)^{2/3} \qquad (2)$$

Fig. 11 shows the variation of strain rate with porosity-corrected stress σ_R (Eq. 2) for the cermets and their associated skeletons, and for TZP. It can be seen that, after the MSA analysis, the three cermets follow the same trend than monolithic zirconia, despite their different nickel contents; skeleton structures also fit adequately to this behavior. This result, also found at the other temperatures studied, corroborates the idea about the ability for carrying load of nickel in Ni20 and Ni30 cermets in contrast with Ni40. In this

percolated cermet, however, nickel plays an important role enhancing the ductility of the composite when compared with its skeleton, as noted previously. The stresses generated by the grain boundary sliding of the zirconia phase can be accommodated by plastic deformation of the continuous nickel phase, which fills the microcracks opened in the matrix avoiding early catastrophic failure (Fig. 12).

It should be noted that data in Fig. 11 lead to an apparent stress exponent n = 3 (the slope of the log $\dot{\varepsilon}$ - log σ curve) over the entire stress range, in contradiction with the values directly measured in the creep tests (Table I) as a function of the local stress (differential method).

The previous analysis shows that the creep rate of TZP-Ni cermets is controlled by the zirconia phase which supports a stress σ_R given by Eq. 2. The continuous variation of n and Q with stress and temperature displayed by high-purity tetragonal zirconia was rationalized on the basis of a single deformation mechanism by grain boundary sliding with n = 2 and Q = 460 kJ·mol^{-1} incorporating a threshold stress σ_o [19]. In the cermets, such a mechanism would lead to a stress dependence of the strain rate of the form $\dot{\varepsilon} \propto (\sigma_R - \sigma_o)^2$. Fig. 13 displays the plots of $\dot{\varepsilon}^{1/2}$ versus σ_R in linear scales at different temperatures, showing the presence of a threshold stress σ_o which decreases with increasing the temperature following the law:

$$\sigma_0 = \frac{4.1 \cdot 10^{-4}}{d} \exp\left(\frac{110\ \text{kJ·mol}^{-1}}{RT}\right), \qquad (3)$$

where σ_0 is in MPa for d in μm.

This expression is in excellent agreement with that reported for monolithic zirconia[19]. The origin of the threshold stress has been related to yttrium segregation at the grain boundaries[19, 33]. It is necessary to remark that the TZP grain boundaries in the cermets show the same characteristics found in high-purity zirconias[34].

5. Summary

The high-temperature plastic behavior of TZP-Ni composites with nickel contents of 20, 30 and 40 vol% has been investigated under compression at constant load in the temperature range 900-1250 ºC in argon atmosphere. The same experiments were performed on ceramic skeletons obtained by chemically removing the metal phase. Below the percolation threshold (34 vol%), the composites consist of isolated nickel particles surrounded by zirconia grains. Above the percolation limit, the cermets are composed by two interconnected continuous phases.

The apparent creep parameters, stress exponent n and activation energy for flow Q, are independent of the nickel content. They change continuously from 5 to 2.5 and from 680 to 490 $kJ \cdot mol^{-1}$, respectively, when decreasing the stress and/or the temperature. These results, also found in the skeletons, indicate that zirconia controls the high-temperature plastic deformation of the cermets.

The strain rates of the cermets are strongly dependent on the percolation of the metal phase. Ni20 and Ni30 exhibit identical deformation rates (three times higher than monolithic TZP), whereas Ni40 is much faster (60 times). A model based on the MSA that takes into account the actual porosity and the volume fraction of percolated nickel leads to a

constitutive equation for creep which is identical to that found for high-purity monolithic zirconia. Ni30 cermets, with a metal content below but very close to the percolation threshold, show a strain-driven transition from non-percolated to percolated behavior.

Acknowledgement

The authors are grateful to Drs. S. López-Esteban and Prof. J. S. Moya (ICMM) for providing the materials for this study and to Dr. M. J. López-Robledo for his kind help.

References

[1]J. E. Sundeen and R. C. Buchanan, "Electrical properties of nickel/zirconia cermet films for temperature- and flow-sensor applications", *Sensor. Actuators A-Phys.*, 63 [1] 33-40 (1997).

[2]H. Hamatani, N. Shimoda, and S. Kitaguchi, "Effect of the composition profile and density of LPPS sprayed functionally graded coating on the thermal shock resistance", *Science and Technology of Advanced Materials,* 4 197-203 (2003).

[3]S. T. Aruna, M. Muthuraman, and K. C. Patil, "Synthesis and properties of Ni-YSZ cermet: anode material for solid oxide fuel cells", *Solid State Ionics*, 111 45-51 (1998).

[4]S.P.S. Badwall, F.T. Ciacchi, and K.M. Giampietro, "Analysis of the conductivity of commercial easy sintering grade 3 mol% Y_2O_3-ZrO_2 materials", *Solid State Ionics*, 176 169-178 (2005).

[5]J. W. Kim, A. V. Virkar, K. Mehta, K.-Z. Fung, and S. C. Singhal, "Low Temperature, High Performance Anode Supported Solid Oxide Fuel Cells", *J. Electrochem. Soc.*, 146 [1] 69-78 (1999).

[6]S. López-Esteban, J. F. Bartolomé, J. S. Moya, and T. Tanimoto, "Mechanical performance of 3Y-TZP/Ni composites: Tensile, bending and uniaxial fatigue tests", *J. Mater. Res.*, 17 [7] 1592-1600 (2002).

[7]A. Morales-Rodríguez, A. Bravo-León, A. Domínguez-Rodríguez, S. López-Esteban, J. S. Moya, and M. Jiménez-Melendo, "High-temperature mechanical properties of zirconia/nickel composites", *J. Eur. Ceram. Soc.*, 23 2849-2856 (2003).

[8]H. Koide, Y. Someya, T. Yoshida, and T. Maruyama, "Properties of Ni/YSZ cermet as anode for SOFC", *Solid State Ionics*, 132 253-260 (2000).

[9]M. Marinsek, K. Zupan K., and J. Macek, "Preparation of Ni-YSZ composite materials for solid oxide fuel cell anodes by the gel-precipitation method", *J. Power Source*, 86 383-389 (2000).

[10]C. Pecharromán, S. López-Esteban, J. F. Bartolomé, and J. S. Moya, "Evidence of Nearest-Neighbor Ordering in Wet-Processed Zirconia-Nickel Composites", *J. Am. Ceram. Soc.*, 84 [10] 2439-41 (2001).

[11]J. P. Poirier, Creep of Crystals, p. 28 Cambridge University Press, Cambridge, 1985

[12]G. Stathis, D. Simwonis, F. Tietz, A. Moropoulou, and A., Naoumides, "Oxidation and resulting mechanical properties of Ni/8Y_2O_3-stabilized zirconia anode substrate for solid-oxide fuel cells", *J. Mater. Res.*, 17 951-958 (2002).

[13]A. Morales-Rodríguez, G. Richter, M. Rühle, A. Bravo-León, A. Domínguez-Rodríguez, and M. Jiménez- Melendo, "Microstructural characteristics of TZP/Ni cermets plastically deformed at high temperature", *J. Eur. Ceram. Soc.*, 27 2053-2059 (2007).

[14]J. A. Hines, Y. Ikuhara, A. H. Chokshi, and T. Sakuma, "The influence of trace impurities on the mechanical characteristics of a superplastic 2 mol% yttria stabilized zirconia", *Acta mater*, 46 [15] 5557-5568 (1998).

[15]S. Stemmer, J. Vleugels, and O. Van Der Biest, "Grain Boundary Segregation in High-purity Yttria-stabilized Tetragonal Zirconia Polycrystals (Y-TZP)", *J. Eur. Ceram. Soc.*, 18 1565-1570 (1998).

[16]A. H. Chokshi, H. Yoshida, Y. Ikuhara, and T. Sakuma, "The influence of trace elements on grain boundary processes in yttria-stabilized tetragonal zirconia", *Mat. Lett.*, 57 4196-4201 (2003).

[17]A. Morales-Rodríguez, A. bravo-León, G. Richter, M. Rühle, A. Domínguez-Rodríguez, and M. Jiménez-Melendo, "Influence of oxidation on the high-temperature mechanical properties of zirconia/nickel cermets", *Scripta Mater.*, 54 2087-2090 (2006).

[18]A. Bravo León, M. Jiménez Melendo, A. Domínguez Rodríguez, and A.H. Chokshi, "The influence of oxygen partial pressure on the creep characteristics of a superplastic 4 mol% yttria partially-stabilized zirconia", *J. Mat Sci. Lett.*, 13 1169-1170 (1994).

[19]M. Jiménez-Melendo, A. Domínguez-Rodríguez, and A. Bravo-León, "Superplastic Flow of Fine-Grained Yttria-Stabilized Zirconia Polycrystals: Constitutive Equation and Deformation Mechanisms", *J. Am. Ceram. Soc.*, 81 [11] 2761-76 (1998).

[20]H. J. Frost and M. F. Ashby, "The F.C.C. metals: Ni, Cu, Ag, Al, Pb and γ-Fe"; pp. 20-24 in Deformation Mechanism Maps: The Plasticity and Creep of Metals and Ceramics. Edited by Pergamon Press. Oxford, UK, 1982.

[21]A. H. Chokshi, "Superplasticity in Fine-Grained Ceramic and Ceramic Composites: Current Understanding and Future Prospects", *Mater. Sci. Eng.*, A166 119-133 (1993).

[22]A. R. de Arellano López, K. C. Goretta, E. T. Park, S. E. Dorris, U. Balchandran, and J. L. Routbort, "High-temperature deformation of a $BaCe_{0.8}Y_{0.2}O_{3-y}$+Ni composite", *J. Eur. Ceram. Soc.*, 22 2555-2560 (2002).

[23]S. Bolognini, G. Feusier, D. Mari, T. Viatte, and W. Benoit, "TiMoCN-based cermets: high-temperature deformation", *Int. J. Refr. Metals Hard Mater.*, 21 19-29 (2003).

[24]J. Martínez Fernández, A. Muñoz, A. R. de Arellano López, F. M. Varela Feria, A. Domínguez-Rodríguez, and M. Singh, "Microstructure-mechanical properties correlation in siliconized silicon carbide ceramics", *Acta Mater.*, 51 [11] 3259-3275 (2003).

[25]D. M. Owen and A. H. Chokshi, ''Final Stage Free Sintering and Sinter Forging Behaviour of a Yttria-Stabilized Tetragonal Zirconia,'' Acta Mater., 46 [2] 719–29 (1998).

[26]F. Wakai, S. Sakaguchi, and Y. Matsuno, “Superplasticity of Yttria-Stabilized Tetragonal ZrO_2 Polyscrystals”, *Adv. Ceram. Mater.*, 1 259-63 (1986).

[27]T. Hermansson and G.L. Dunlop, “A High-Temperature Tensile Testing Rig for Ceramic Materials”, *Int. J. High Technol. Ceramic.*, 4 263-68 (1988).

[28]J. D. French, J. Zhao, M. P. Harmer, H. M. Chan, and G. A. Miller, “Creep of duplex microstructures”, *J. Am. Ceram. Soc.*, 77 [11] 2857-2865 (1994).

[29]R. W. Rice, “Evaluation and extension of physical property-porosity models based on minimum solid area”, *J. Mater. Sci.*, 31 102-118 (1996).

[30]R. W. Rice; pp. 72-76 in *Porosity of ceramics*. Edited by M. Dekker Inc. New York, USA, 2000.

[31]D. Sotiropoulou and S. Ladas, “An XPS and XAES study of the Ni/ZrO_2 interface”, *Surface Science*, 408 182-189 (1998).

[32]A. Tsoga, A. Naoumidis, and P. Nikolopoulus, “Wettability and interfacial reactions in the systems Ni/YSZ and Ni/Ti-TiO_2/YSZ”, *Acta mater.*, 44 [9] 3679-3692 (1996).

[33]A. Domínguez-Rodríguez, D. Gómez-García, C. Lorenzo-Martín, and A. Muñoz-Bernabé, “Influence of the yttrium segregation at grain boundaries in the superplasticity of yttria tetragonal zirconia polycrystals”, *J. Eur. Ceram. Soc.*, 23 2969-2973 (2003).

[34]T. Ikuhara, P. Thavorniti, and T. Sakuma, “Solute segregation at grain boundaries in superplastic SiO_2-doped TZP”, *Acta mater.*, 45 [12] 5275-5284 (1997).

Figure 1

Fig. 1. Scanning electron microscopy (SEM) micrographs of as-received cermets: (A) Ni20, (B) Ni30, and (C) Ni40. Overlapping between neighbor nickel particles occurs in Ni40. The inset shows the fine-grained microstructure of the zirconia matrix

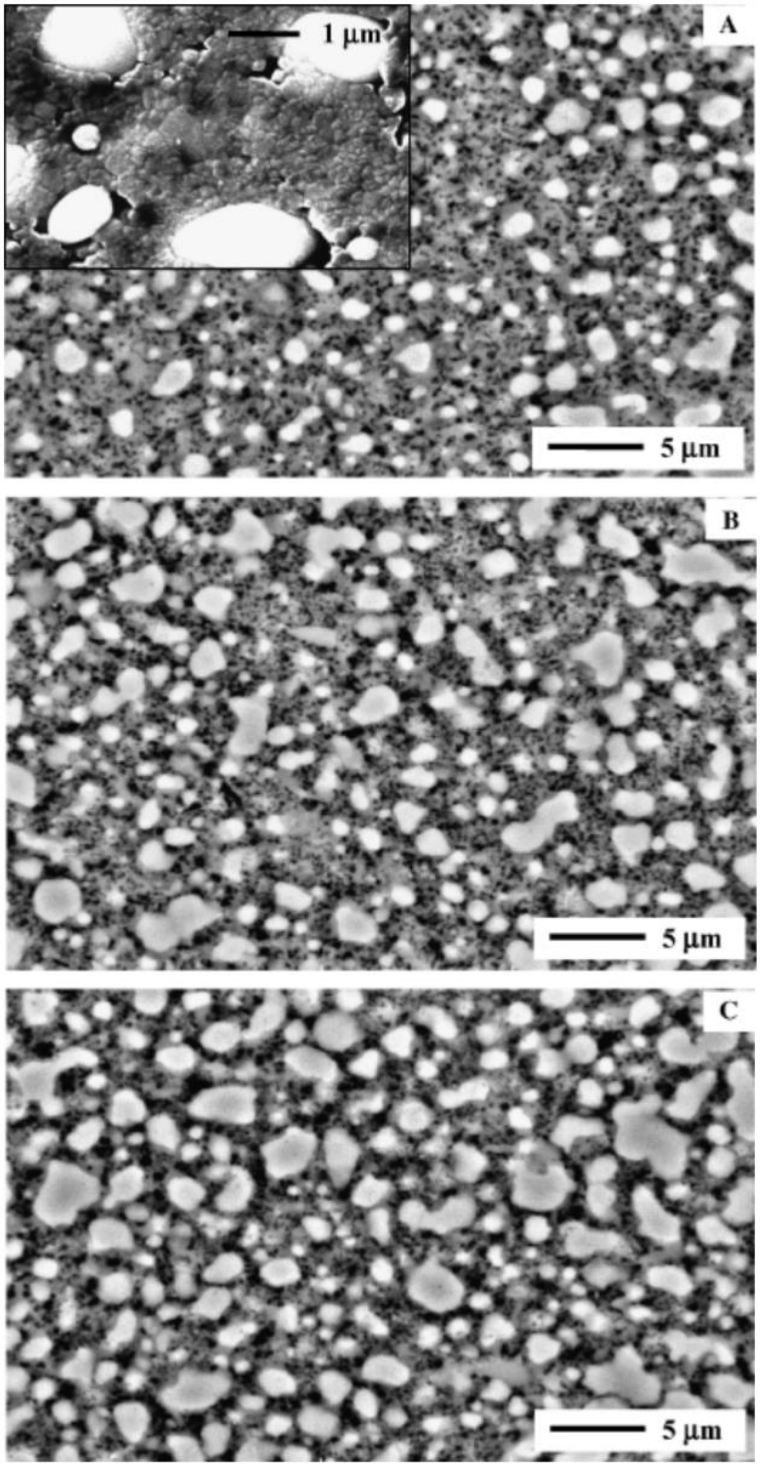

Figure 2

Fig. 2. Scanning electron microscopy (SEM) micrographs of (A) Ni20 and (B) Ni40 ceramic skeletons obtained by chemical etching of the cermets.

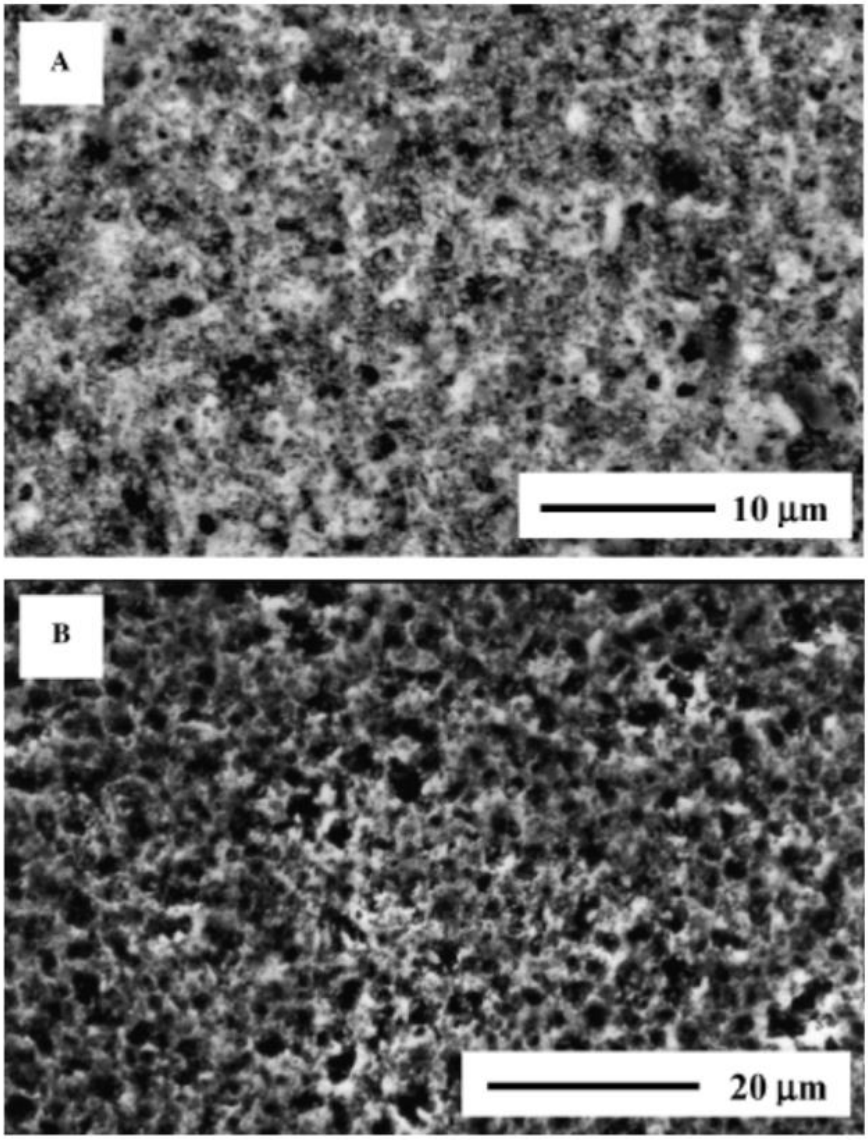

Figure 3

Fig. 3. Low-magnification scanning electron microscopy (SEM) micrographs of an Ni20 cermet: (A) as received; (B) strained ε = 45% at 1250 °C and stresses up to 14 MPa. The compression axis is vertical.

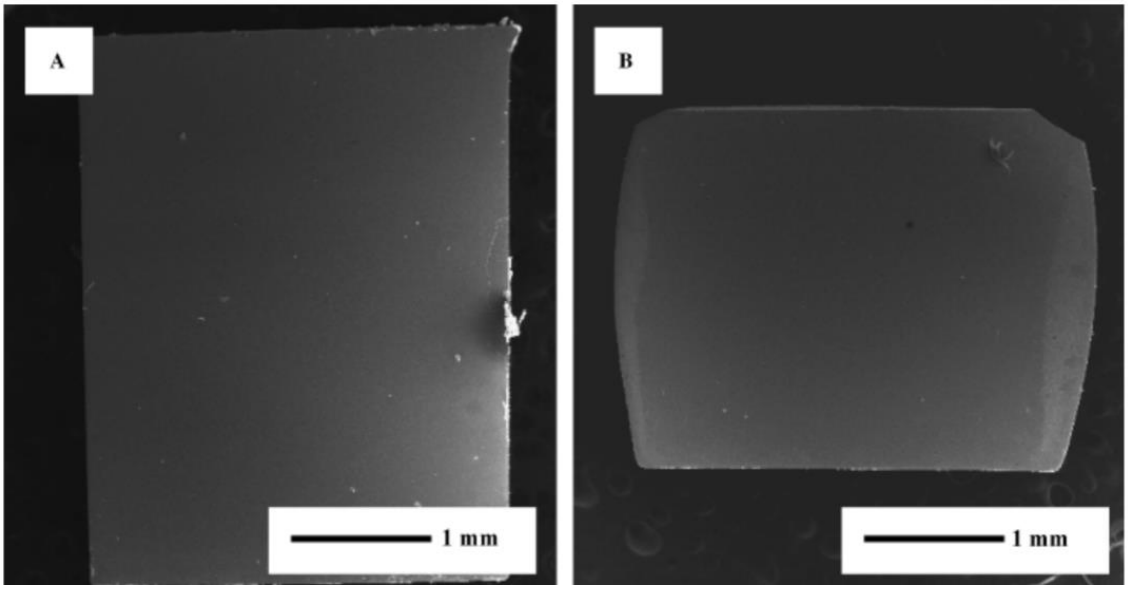

Figure 4

Fig. 4. Creep curves at 1200 °C–1250 °C and low stresses for Ni20, Ni30, and Ni40. Several determinations of the apparent stress exponent n and activation energy Q by stress and temperature changes are shown. The same values of n and Q were measured for the three cermets (not shown for the sake of clarity, see text).

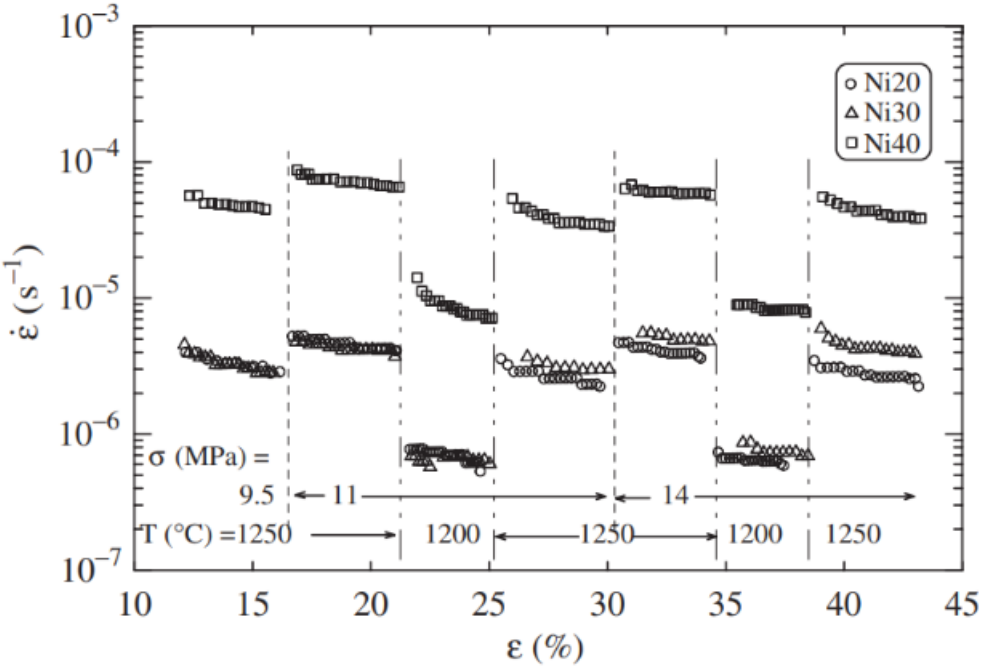

Figure 5

Fig. 5. Creep curves for Ni20 and Ni30 at 1250 ºC and σ = 20 MPa. The strain rates are identical at the first stages of deformation but diverge when strain progresses.

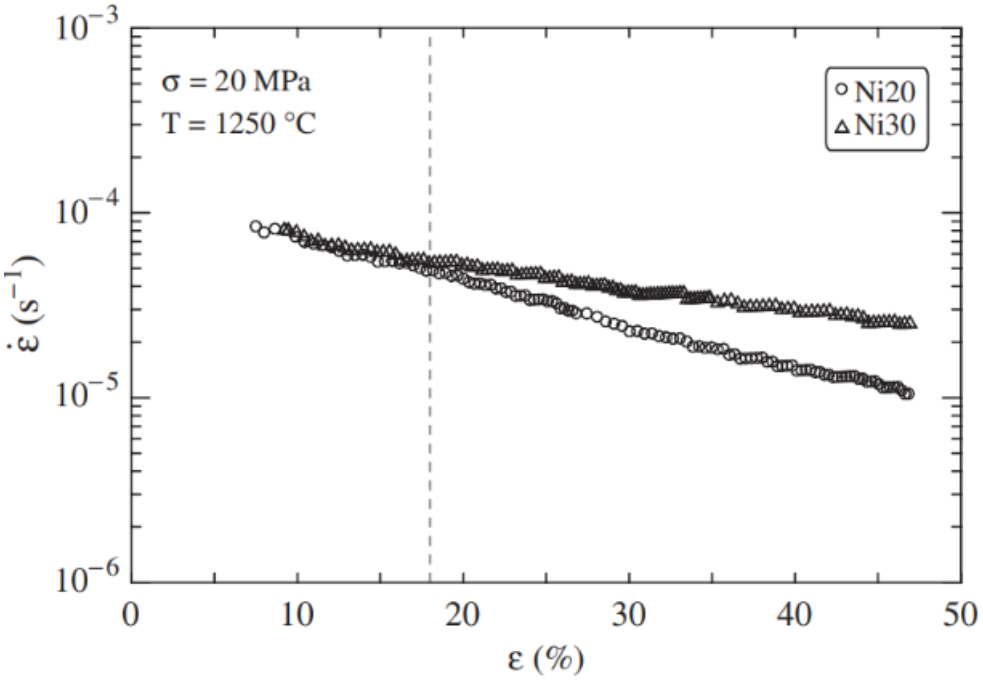

Figure 6

Fig. 6. Creep curve for Ni40 at 1150 ºC –1200 ºC and intermediate stresses. Average values of n = 4.9 and Q = 660 kJ/mol were measured.

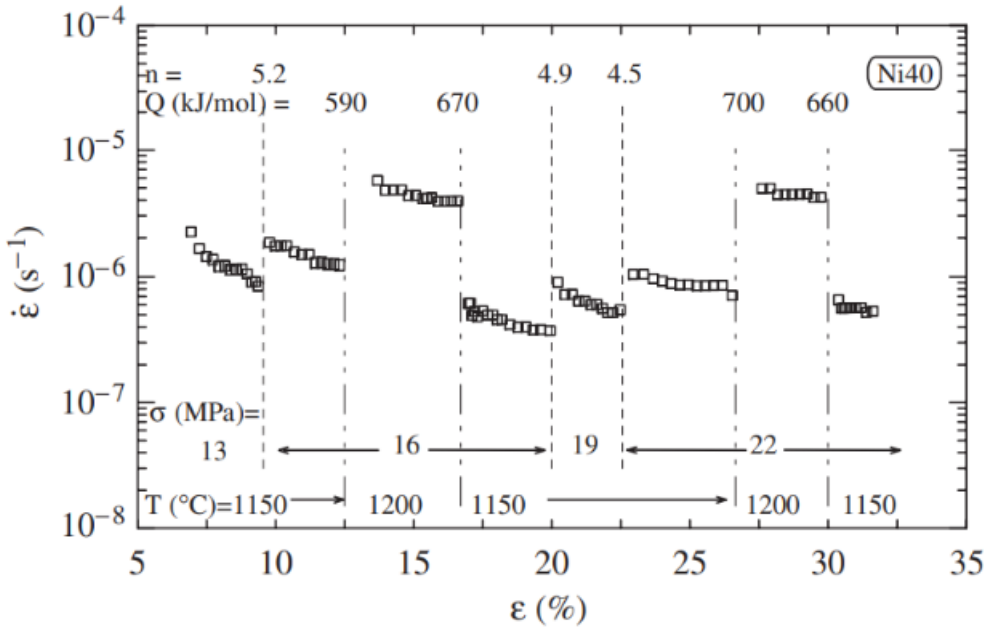

Figure 7

Fig. 7. Creep curves of Ni20 and Ni40 cermets and their associated skeletons. The same average values n = 4.1 ± 0.3 and Q = 660 ± 20 kJ·mol^{-1} were found for the four materials.

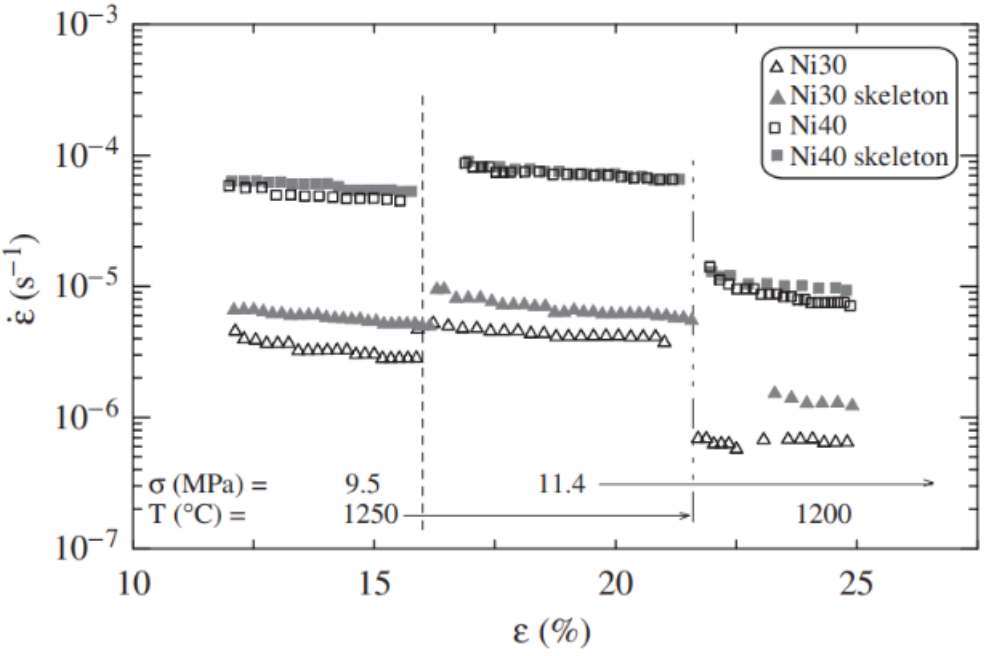

Figure 8

Fig. 8. SEM micrographs of cermets deformed up to 45%: (A) Ni20, (B) Ni30 and (C) Ni40. The compression axis is vertical.

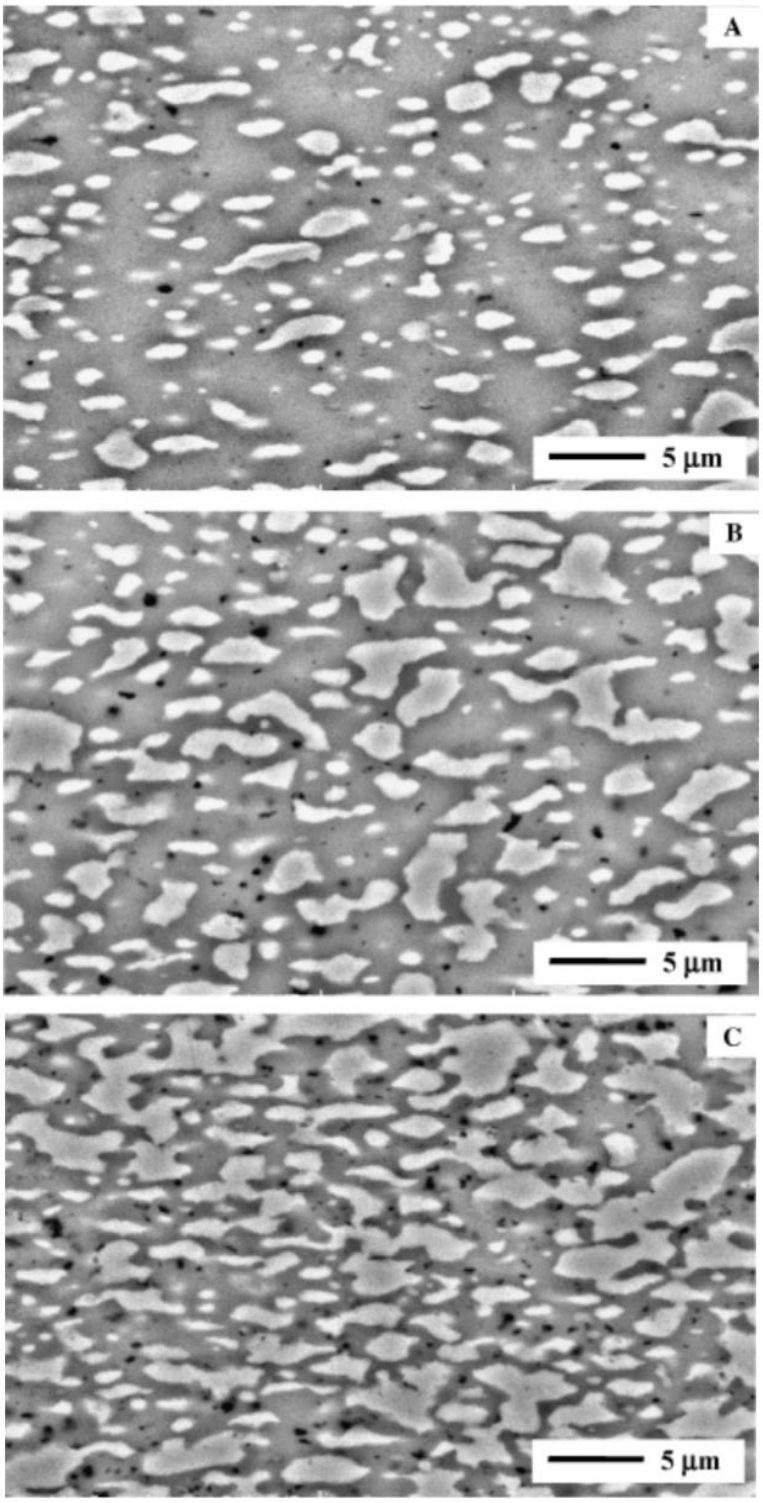

Figure 9

Fig. 9. SEM micrograph of Ni20 deformed at high stresses. Occasional microcracks by cavity coalescence can be observed. The compression axis is vertical.

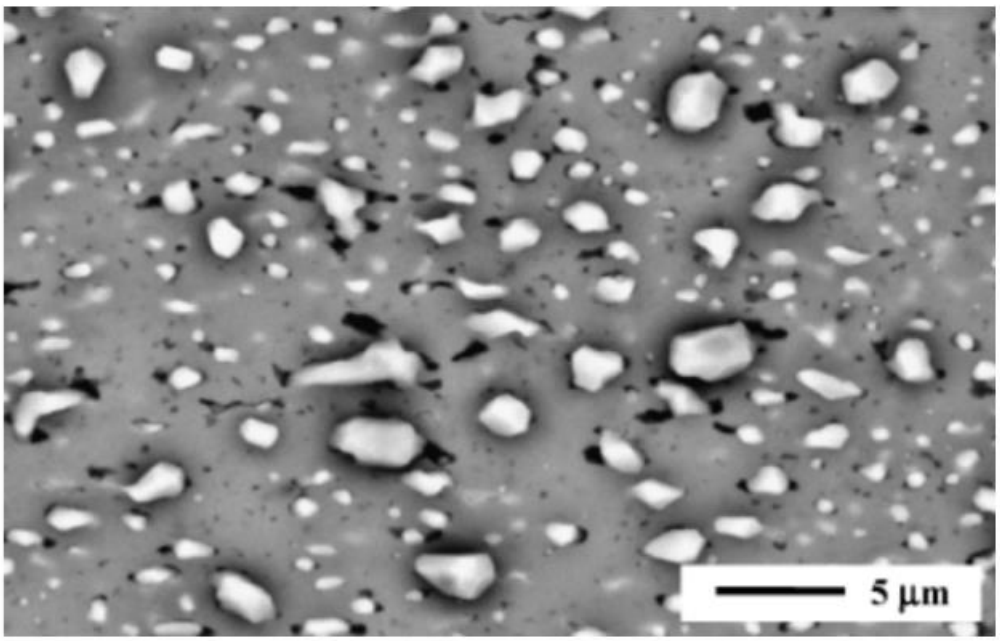

Figure 10

Fig. 10. Variation of grain size compensated strain rate $\dot{\varepsilon}_0$ (ε = 0) with stress at 1250 °C for cermets and monolithic zirconia. Data reported for high-purity TZP[26,27] are also shown. The dashed line represents the prediction for TZP with n = 2.[19]

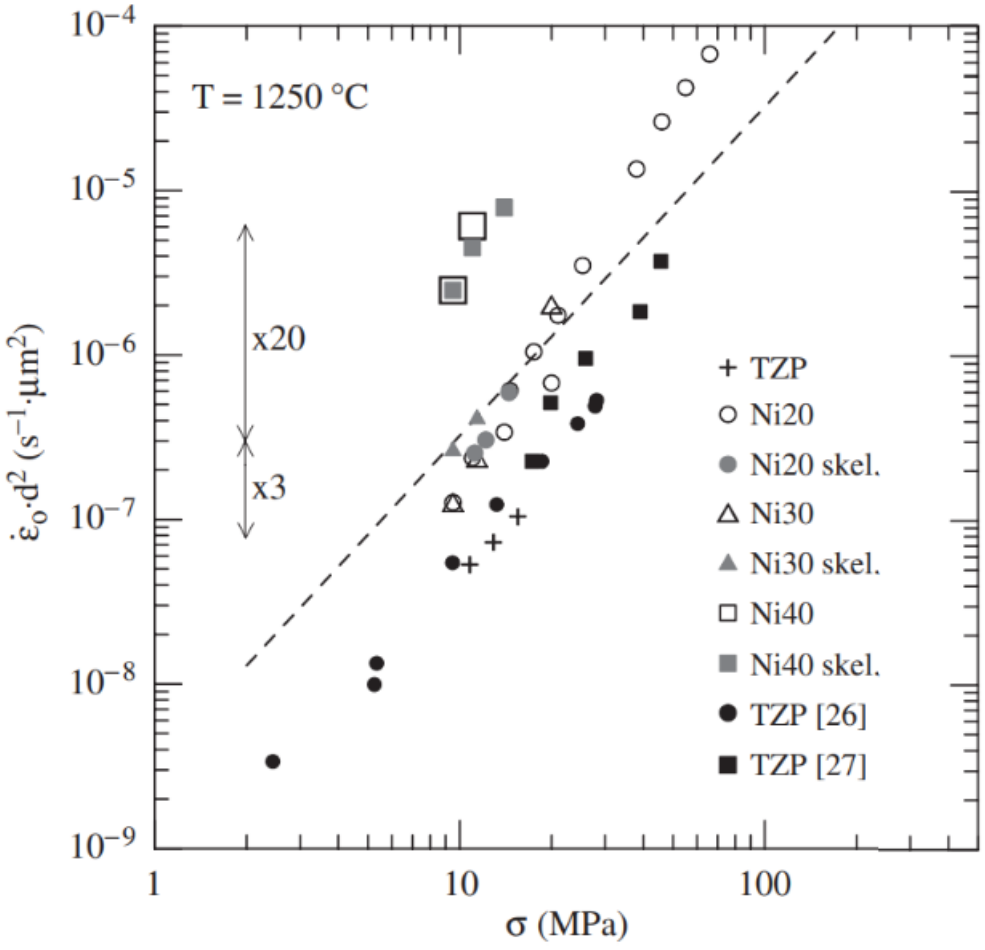

Figure 11

Fig. 11. Variation of strain rate $\dot{\varepsilon}_0$ with porosity-corrected stress Eq. (2) for the cermets and their associated skeletons, as well as monolithic TZP.

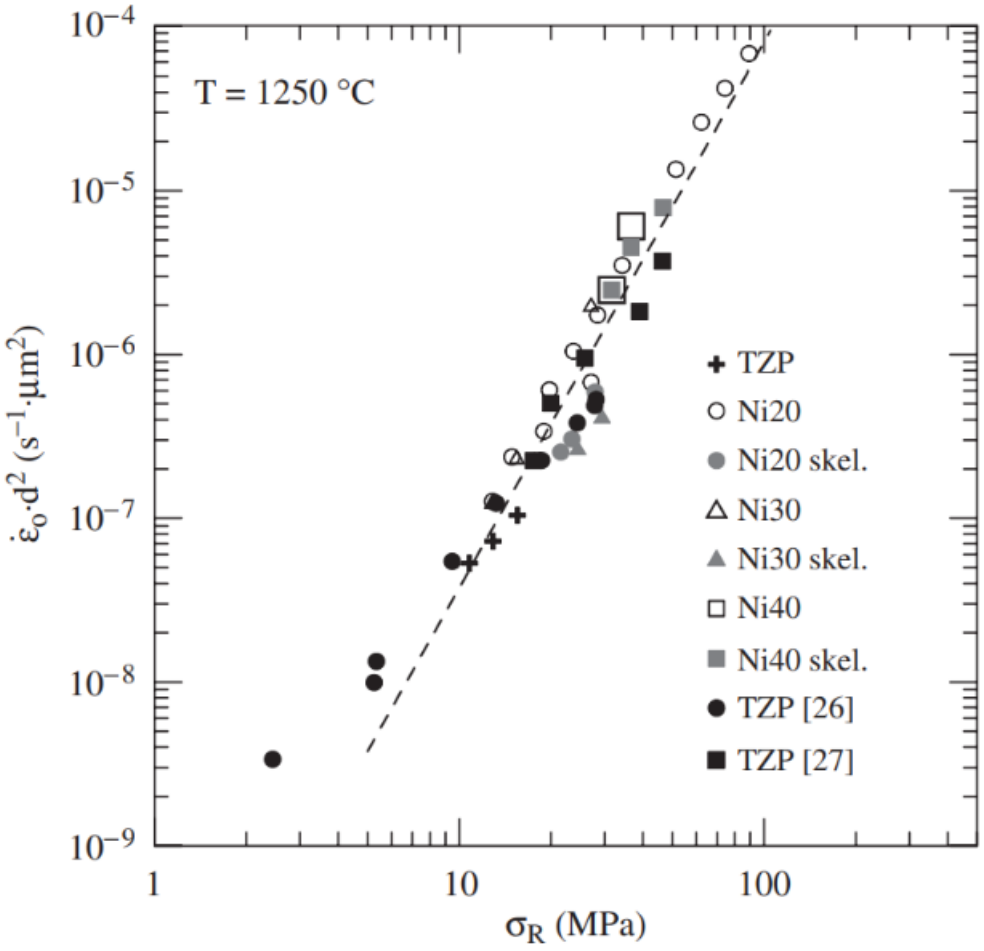

Figure 12

Fig. 12. Scanning electron microscopy (SEM) micrograph of Ni40 deformed at 950 ºC (ε = 30%). The metal phase fills the microcracks opened in the zirconia matrix, enhancing the composite ductility.

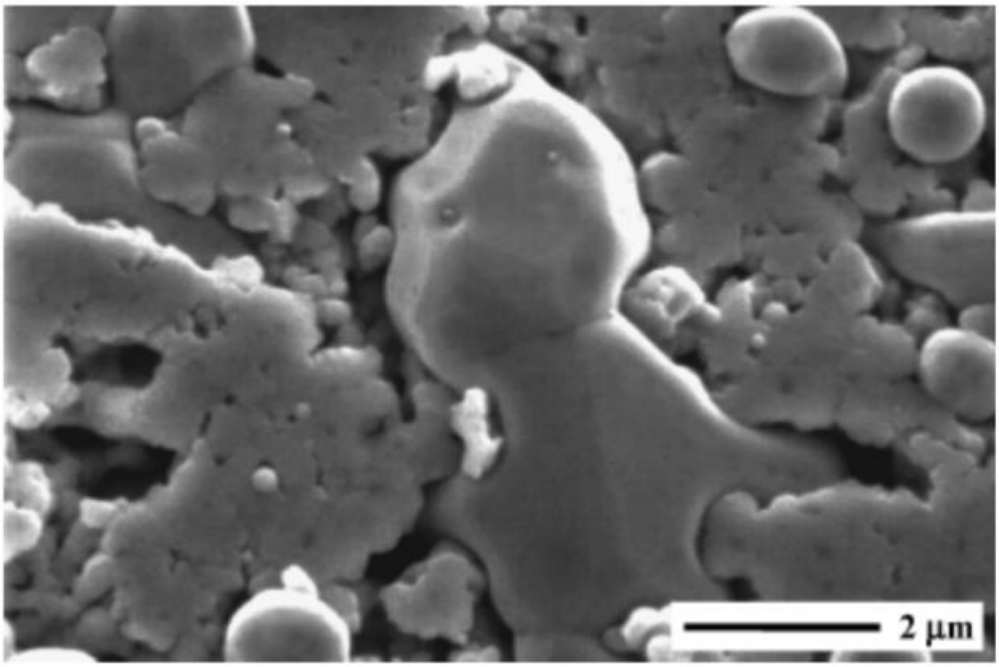

Figure 13

Fig. 13. Variation of $\dot{\varepsilon}_0^{1/2}$ with porosity-corrected stress for TZP-Ni cermets at various temperatures, showing the presence of a threshold stress that decreases with increasing the temperature.

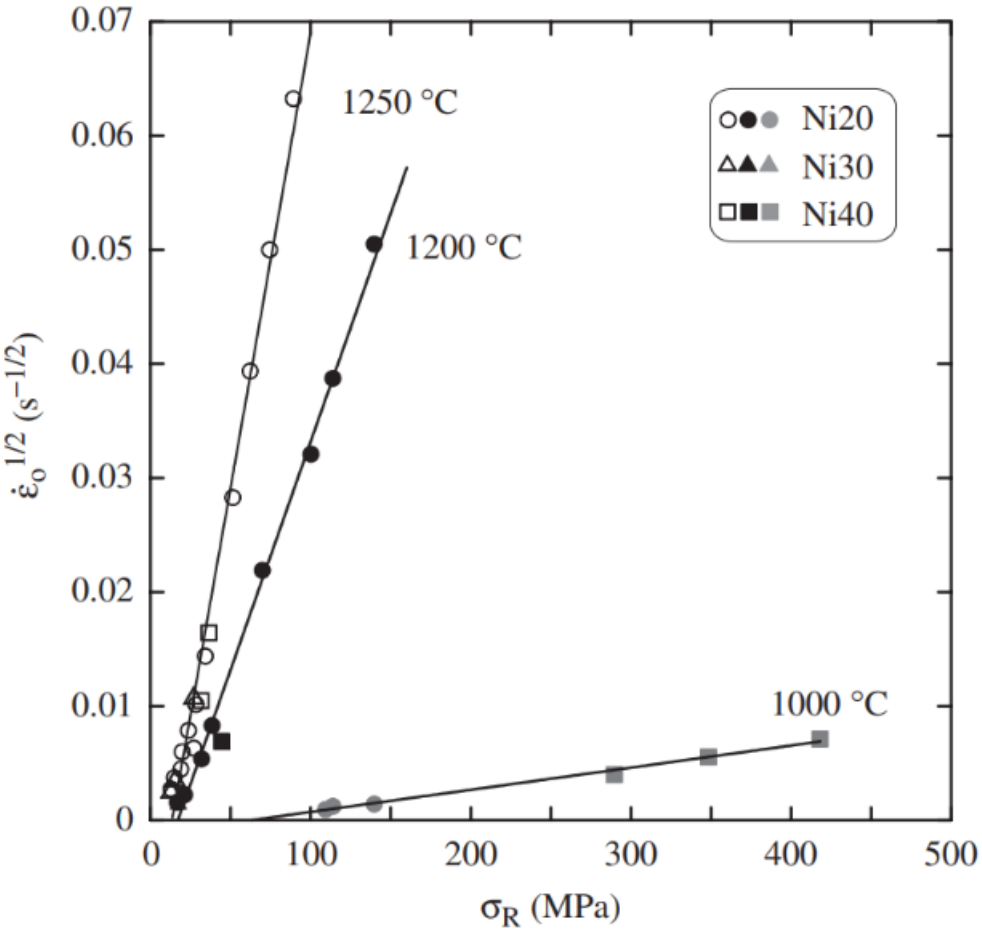

Table I

Table I. Stress exponent n calculated for TZP-Ni cermets in argon atmosphere under different experimental conditions.

T (ºC)	σ (MPa)	Material	N
1250	11 - 16	TZP	2.9 ± 0.1
	9 - 14	Ni20	4.0 ± 0.4
	9 - 14	Ni30	3.8 ± 0.5
	9 - 14	Ni40	3.9 ± 0.1
	15 - 25	Ni20	3.5 ± 0.2
	32 - 66	Ni20	2.8 ± 0.3
1200	75 – 92	Ni20	2.9 ± 0.1
	32 - 66	Ni20	3.0 ± 0.4
1150	32 - 66	Ni30	2.5 ± 0.2
	13 - 22	Ni40	4.9 ± 0.3
1050	60 - 125	Ni20	3.0 ± 0.2
	60 – 72	Ni40	2.5 ± 0.3
1000	75 – 92	Ni20	2.9 ± 0.3
	72-104	Ni40	2.6 ± 0.1
950	100 – 144	Ni40	2.6 ± 0.1

Ni20, TZP-20 vol% Ni; Ni30, TZP-30 vol% Ni; Ni40, TZP-40 vol% Ni; TZP, tetragonal zirconia.

Table II

Table II. Activation energy for flow Q calculated for TZP-Ni cermets in argon atmosphere under different experimental conditions.

T (ºC)	σ (MPa)	Material	Q (kJ·mol^{-1})
1250 - 1200	11 - 14	Ni20	620 ± 20
	21 - 25		550 ± 30
	46 - 66		490 ± 50
	11 - 14	Ni30	670 ± 60
	11 - 14	Ni40	640 ± 50
1000 - 1200	75	Ni20	530 ± 50
1100 - 1200	75	Ni20	530 ± 50
1150 - 1200	16 - 22	Ni40	660 ± 50
1150 - 1100	44 - 66	Ni20	650 ± 50
	44 - 66	Ni30	550 ± 40
1050 - 1000	72	Ni20	670 ± 70
	72	Ni40	650 ± 20
1000 - 950	80	Ni40	640 ± 60
	104		630 ± 20
950 - 900	144	Ni40	670 ± 40

Ni20, TZP-20 vol% Ni; Ni30, TZP-30 vol% Ni; Ni40, TZP-40 vol% Ni; TZP, tetragonal zirconia.